J Infrared Milli Terahz Waves (2009) 30:294–301
DOI 10.1007/s10762-008-9446-6

Analysis of Rectangular Folded-Waveguide Millimeter-Wave Slow-wave Structures using Conformal Transformations

M. Sumathy · K. J. Vinoy · S. K. Datta

Received: 10 June 2008 / Accepted: 11 November 2008 /
Published online: 29 November 2008

Abstract An analysis of rectangular folded-waveguide slow-wave structure was developed using conformal mapping technique through Schwarz's polygon transformation and closed form expressions for the lumped capacitance and inductance per period of the slow-wave structure were derived in terms of the physical dimensions of the structure, incorporating the effects of the beam hole in the lumped parameters. The lumped parameters were subsequently interpreted for obtaining the dispersion and interaction impedance characteristics of the structure. The analysis was benchmarked for two typical millimeter-wave structures, one operating in Ka-band and the other operating in Q-band, against measurement and 3D electromagnetic modeling using MAFIA.

Keywords Conformal mapping · Conformal transformation · Polygon transformation · Rectangular folded-waveguide (RFW) · Slow-wave Structure (SWS) · Traveling-wave tube (TWT)

Abbreviations
RFW Rectangular folded-waveguide
SWS Slow-wave structure
TWT Traveling-wave tube

1 Introduction

Rectangular folded-waveguide slow-wave structures show promises for millimeter-wave traveling-wave tubes (TWTs) with its potential for reasonably broadband, high power

M. Sumathy (✉) · S. K. Datta
Microwave Tube Research and Development Centre, Bharat Electronics Complex,
Jalahalli Post, Bangalore 560013, India
e-mail: msumti@yahoo.co.in

K. J. Vinoy
Department of Electronics & Communication Engineering, Indian Institute of Science,
Bangalore 560054, India

operation and ease of fabrication as well. A typical schematic of a rectangular folded-waveguide slow-wave structure is shown in Fig. 1. Each period of the folded-waveguide structure consists of two wave-guide elements: (i) a straight rectangular waveguide section (having broad-dimension a and narrow-dimension b) accommodating the beam hole as apertures at the broad-wall, and (ii) an E-plane straight-section. An electron beam passing through the beam-hole interacts with the axial electric field having fundamental TE_{10} mode configuration. The polarity of the electric field reverses at each E-plane bend with respect to the electron beam velocity. By design, the rate of change of phase of the axial electric field is made to synchronize with the electronic phase of the electron beam to facilitate the beam-wave interaction. The phase-shift per period of the structure is such that the structure belongs to the fundamentally backward wave circuits like a conventional coupled-cavity slow-wave structure.

There is a surge of recent activities observed in the area that reveal concerted efforts in harnessing the potentials of the folded-waveguide slow-wave structure towards development of millimeter-wave TWTs [1–4], where the emphasis was shown to design using commercially available 3D electromagnetic codes. However, as far as the authors are aware, the analytical approach in this regard has been a bit neglected in the published domain of literature, except some pioneering efforts by Hyun *et al.* [5], Carter [6] and Seong *et al.* [7]. Approach of Hyun *et al.* [5] proposes a simple waveguide analysis ignoring the contributions of the beam hole. A method to synthesize the parameters of a rectangular straight bend folded-waveguide traveling-wave tube such as dispersion, interaction impedance and growth rate were derived and the results were benchmarked with numerical simulation by HFSS by Seong *et al.* [7], again ignoring the effects of the beam-hole. An improved equivalent circuit model of a rectangular straight-bend folded-waveguide slow-wave structure excluding the beam hole effect was reported by Carter [6] using cascaded transmission line approach, in which right angled bends were described by equivalent circuits for which the lumped parameters were computed directly from the dimensions of the slow-wave structure.

In the present work, we propose an exact analysis of a rectangular folded-waveguide slow-wave structure by conformal mapping using Schwarz Christoffel transformation [8] following the approach suggested by Erich Glass for circular cylindrical cavities [9] used in

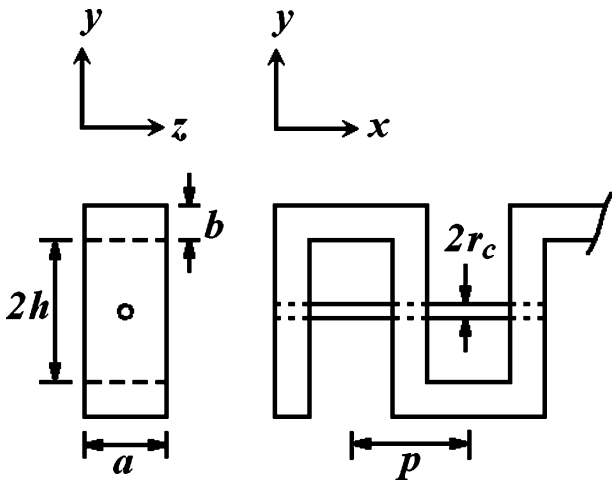

Fig. 1 Schematic of a typical straight bend folded-waveguide slow-wave structure showing the relevant dimensions.

a coupled-cavity traveling-wave tube. The closed form expressions for the lumped parameters of the structure such as inductance per period and capacitance per period of the slow-wave structure were derived in terms of the physical dimensions of the structure. The effect of beam hole was also included in the analysis, by considering it as a circular aperture at the broad-wall of the rectangular waveguide centered at the location of electric field maxima. The analysis has been carried out in three steps: first, the longitudinal profile of the rectangular folded-waveguide slow-wave structure without considering its depth is modeled as a polygon in *Z*-plane ($Z(x, y)$) and Schwartz's polygon transformation is used for an intermediate mapping (Fig. 2) to a linear domain (*T*-plane: $T(r, s)$). Next, the linear domain is mapped to a parallel line domain having 2-unit width and a specific distance between two lines (*W*-plane: $W(u, v)$). The *W*-plane values are used for calculating the capacitance and inductance of the structure. Finally, the effects of the presence of beam hole are included in the lumped circuit parameters following the approach of Booske *et al.* [10] as used for serpentine folded-waveguide slow-wave structures. The lumped parameters were subsequently interpreted to obtain the dispersion and interaction impedance characteristics of the structure. The analysis was benchmarked for the dispersion and interaction impedance characteristics against those from 3D electromagnetic modeling using MAFIA for two typical millimeter-wave structures, one operating in Ka-band and the other operating in Q-band.

2 Analysis

The present analysis uses the Schwarz Christoffel transformation for general polygon, that transforms the interior of a polygon in the *Z*-plane into the upper-half of another plane (*T*-plane) in such a manner that the sides of the polygon transform into straight-line segments on the real axis of the *T*-plane [8, 9]. For analyzing one period of the slow-wave structure,

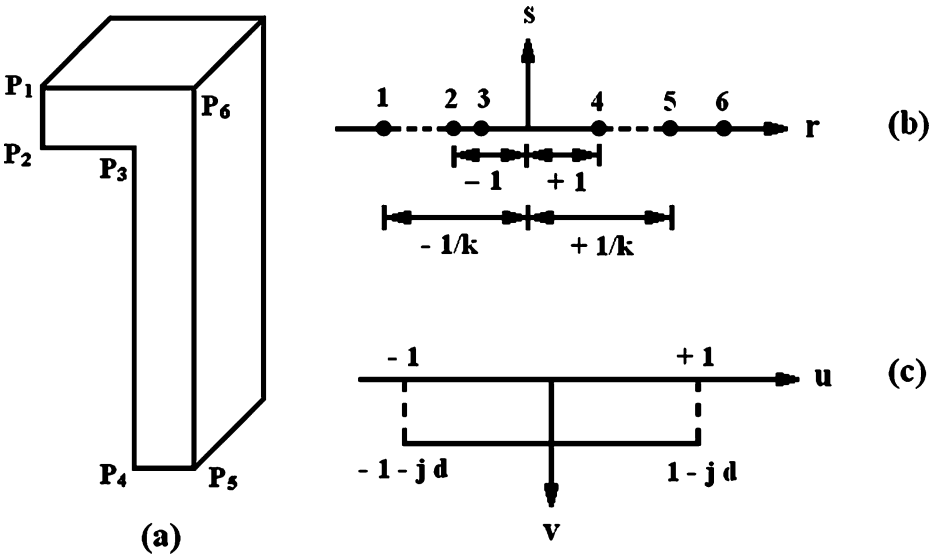

Fig. 2 One half period of the straight bend Folded waveguide SWS (a) in *Z*-plane, (b) in *T*-plane and (c) transformed from *T*-plane to *W*-plane.

we applied the polygon transformation to a half period of the structure (Fig. 2(a)) as it can reconstruct the full period by geometrical method of inversion and reflection. The *Z*-plane polygon has 6 vertices (P_1, P_2.....P_6) with 6 interior angles (α_1, α_2 .....α_6), that transforms line-segments into a straight-line $s=0$ in the *T*-plane, such that $P_n \rightarrow r_n$ as shown in Fig. 2(b) conserving the continuity and analyticity of the transformation function given as:

$$\frac{dZ}{dT} = A\prod_{n=1}^{6}(T-r_n)^{\left(\frac{\alpha_n}{\pi}-1\right)} \tag{1}$$

Here, the domain variables are defined as $Z=x+jy$ and $T=r+js$. The constant 'A' is a complex constant, r_n and α_n are real numbers ($r_1<r_2<....r_6$). One can now easily assign the values of the interior angles (α_n), in the *Z*-plane, following the direction of the sides of the polygon with respect to the *x*-axis, and also the transformed co-ordinates of the vertices in the *T*-plane, in terms of a real variable *k*. The variable is chosen such that the subsequent transformations would take convenient form for mathematical derivations. The boundary of the 2D-section (Fig. 2(a)) can be mapped into the real axis in the *T*-plane, covering the entire *r*-axis, as:

$$\begin{array}{lllll}
P_1: & Z=-b+jh+b & \alpha_1=-\frac{\pi}{2} & T=\frac{1}{k} \\
P_2: & Z=-\frac{b}{2}-\frac{p}{2}+jh & \alpha_2=-\frac{\pi}{2} & T=-1 \\
P_3: & Z=-b+jh & \alpha_3=\frac{\pi}{2} & T=r_3 \\
P_4: & Z=-b & \alpha_4=-\frac{\pi}{2} & T=1 \\
P_5: & Z=0 & \alpha_5=-\frac{\pi}{2} & T=\frac{1}{k} \\
P_6: & Z=j(h+b) & \alpha_6=-\frac{\pi}{2} & T=r_6=\infty
\end{array} \tag{2}$$

Here, the vertices defined above are chosen from experience such that the boundaries in the *Z*-plane could be easily transformed into line-segments in the *T*-plane, without affecting the continuity of the boundaries in the *Z*-plane to *T*-plane. Applying the transformations of the points, we get the simplified transformation function as [9]:

$$\frac{dZ}{dT} = A\left(\frac{\sqrt{\frac{T-r_3}{T-r_6}}}{\sqrt{(T^2-1)\left(T^2-\frac{1}{k^2}\right)}}\right) \tag{3}$$

which on integration yields the relation between the transformed variables that would be used in the next step of conformal transformation to W-plane, given as:

$$Z = A\int\left(\frac{\sqrt{\frac{T-r_3}{T-r_6}}}{\sqrt{(T^2-1)\left(T^2-\frac{1}{k^2}\right)}}\right)dT + B \tag{4}$$

Evaluation of the real variable (*k*) is carried out by substituting the transformed vertices in (4) and eliminating A, B, r_3 and r_6 as:

$$k = \frac{2}{\exp\left(\frac{h+b}{p+b}\right)+\exp\left(-\frac{h+b}{p+b}\right)} \tag{5}$$

Next step is to map r-axis in the T-plane into a rectangle in the W-plane, as shown in Fig. 2(c), for which let us assign the transformed points as,

$$\begin{array}{ll} T=0, & W=0 \\ T=\frac{1}{k}, & W=1 \\ T=-\frac{1}{k}, & W=-1 \\ T=1, & W=1-jd \end{array} \tag{6}$$

with the corresponding mapping function as,

$$W=\mathrm{A}_1\int\frac{1}{\sqrt{\left(T^2-\frac{1}{k^2}\right)}(T^2-1)}+\mathrm{B}_1 \tag{7}$$

The integrand in (7) is an inverse elliptic function, which on integration yields the mapping function in terms of incomplete elliptical integral of first-kind [8], as:

$$W=\mathrm{A}_1\,sn^{-1}(tk,k)+\mathrm{B}_1 \tag{8}$$

Substitution of the values of transformed points from T-plane to W-plane (6), in the mapping function (8), results in three simultaneous equations involving three unknowns A_1, B_1 and d, which on solving give,

$$d=\frac{K}{K'}=\frac{K(k')}{K(k)} \tag{9}$$

with

$$K=sn^{-1}(1,k), \qquad K-jK'=sn^{-1}\left(\tfrac{1}{k},\ k\right)$$
$$k'=\sqrt{1-k^2}, \qquad \text{and} \quad k=\frac{2}{\exp\left(\frac{h+b}{p+b}\right)+\exp\left(-\frac{h+b}{p+b}\right)}$$

The values of the incomplete elliptical integral of first-kind are evaluated with the help of the following expressions as [8]:

$$\frac{K(k)}{K(k')}\cong\frac{\pi}{\ln\left[\frac{2\left(1+\sqrt{k'}\right)}{\left(1-\sqrt{k'}\right)}\right]} \qquad 0\le k\le 0.707, \quad 0\le\frac{K(k)}{K(k')}\le 1 \tag{10}$$

$$\frac{K(k)}{K(k')}\cong\frac{1}{\pi}\ln\left[\frac{2\left(1+\sqrt{k}\right)}{\left(1-\sqrt{k}\right)}\right] \qquad 0.707\le k\le 1, \quad 1\le\frac{K(k)}{K(k')}\le\infty \tag{11}$$

Thus, the 2D geometry of half-period of the rectangular folded-waveguide slow-wave structure is finally mapped to the W-plane as a capacitor of 2-unit length (with plate width of a) having plate separation d. One can now easily express the lumped circuit capacitance per period by cascading two such half periods, as:

$$C_W=\frac{\varepsilon_0\,(2a\times 1)}{d}=2a\varepsilon_0\frac{K(k)}{K(k')} \tag{12}$$

Subsequently, from the TEM-wave consideration in the W-plane, the resonant wavelength of the structure is considered as twice the circuit length [11], and thus, at resonance, the lumped circuit inductance per period is expressed as:

$$L_W=\left(\frac{2\pi\mu_0}{\pi^2}\right)\left(\frac{K(k')}{K(k)}\right) \tag{13}$$

Now, we seek to incorporate the contributions of the beam hole to the lumped circuit parameters, which is accomplished by considering the beam hole as a circular aperture at the broad-wall of the rectangular waveguide centered at the location of maximum electric field, the diameter of the aperture ($2r_c$) being small enough to support no propagating mode at the operating frequency. Thus, we treated the aperture as a stub at the broad-wall [10, 12], and the corresponding lumped circuit parameters for the apertures are expressed as:

$$\begin{aligned} L_H &= \frac{\pi M \lambda_g}{\omega^2 \lambda^2 ab\left(1-\frac{2\pi M}{\lambda^2 b}\right)} \\ C_H &= \frac{2\pi}{Y_0 \omega \lambda_g ab\left(\frac{1}{M}-\left(\frac{\pi}{a^2 b}+\frac{7.74}{2\pi r_c^3}\right)\right)} \end{aligned} \tag{14}$$

Here, Y_0 is the wave-admittance of the rectangular waveguide, λ_g is the guide wavelength, and $M\,(=r_c^3/6)$ is an empirical factor [10, 12]. With this correction, the total lumped circuit inductance and capacitance for a period of the rectangular folded-waveguide slow-wave structure are given as:

$$\begin{aligned} L &= L_W + L_H \\ C &= C_W + C_H \end{aligned} \tag{15}$$

Subsequently, using the expressions of inductance and capacitance per period of the structure, one can easily express the space-harmonic phase shift (β_m) and the interaction impedance (K) of the slow-wave structure following the approach of Carter and Liu [11] given as:

$$\beta_m = \frac{\omega_s^2 - \omega^2}{c^2}\left(1+\frac{L}{P}\right) + \frac{m\pi}{P} \tag{16}$$

$$K = \sqrt{\frac{L}{C}}\frac{1}{(\beta_m P)^2}\left(\frac{\sin \beta_m b/2}{\beta_m b/2}\right)^2 \tag{17}$$

$$\text{with } \omega_s = 1/\sqrt{LC}$$

3 Results and discussion

For numerical appreciation of the problem, we considered two typical millimeter-wave rectangular folded-waveguide slow-wave structures operating in forward space-harmonic mode: one operating in Ka-band and the other operating in Q-band. The Ka-band structure uses a non-standard rectangular waveguide around WR-28, designed such that the coupling structures could be made compatible to standard WR-28 waveguide measurement set up. Similarly, the Q-band structure also was designed using a non-standard rectangular waveguide around WR-15. The dispersion and interaction impedance characteristics of these structures were evaluated using present approach and compared to those from 3D electromagnetic modeling in MAFIA. The 3D electromagnetic modeling in MAFIA was carried out following eigen-mode analysis for a 2-period structure having periodic boundaries and the dispersion and interaction impedance values at the eigen-frequencies were computed following the approach of Booske *et al.* [10].

The Ka-band structure was further benchmarked against measurement. The structure was fabricated using wire-EDM technique and the dispersion and interaction impedance

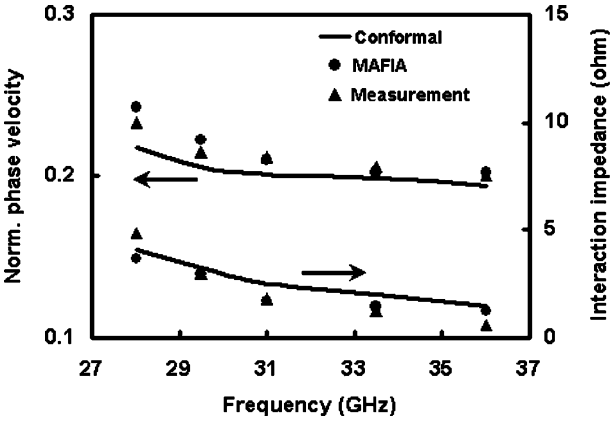

Fig. 3 Dispersion and Interaction Impedance characteristics of the Ka-band structure and its benchmarking with measurement and MAFIA simulation. The structure uses a non-standard WR-28 waveguide with a/p=3.68, b/p=0.364, h/p=1.84 and r_c/p=0.165.

characteristics were measured using non-resonant perturbation technique proposed by Genack *et al.* [13]. The dispersion and interaction impedance characteristics of the above structures as analyzed using the present approach vis-à-vis their benchmarking with measurement (only for the Ka-band structure) and MAFIA modeling are presented in Fig. 3 and Fig. 4.

It may be noted that the analytical prediction of dispersion characteristics show lesser accuracy at lower frequencies close to the cut-off mode of the structure where the phase-shift per period becomes close to π. This may be attributed to the limitations of conformal transformations that the method considers the field distribution over a cross-sectional plane of a waveguide as a static field distribution [14], and moreover the homogeneity of the static field distribution deteriorates at the bent portion of the waveguide around the π-phase-shift frequency [9] breaking the basic assumption of the conformal transformation, thereby reducing the accuracy in prediction at the lower frequencies close to the π-phase-shift frequency. However, as observed for both the Ka-band and the Q-band structures, one may expect a fairly reasonable accuracy in computation of dispersion and interaction impedance characteristics around the regime of operation of this type of slow-wave structures where the phase-shift per period is close to 1.5π.

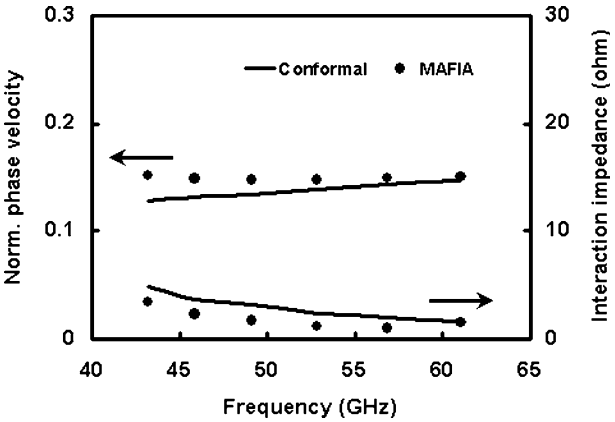

Fig. 4 Dispersion characteristics of the Q-band structure and its benchmarking with MAFIA simulation. The structure uses a non-standard WR-15 waveguide with a/p=5.41, b/p=0.541, h/p=2.71, and r_c/p=0.214.

4 Conclusion

An exact analytical treatment for rectangular folded-waveguide slow-wave structure including the effects of the beam-hole has been carried out following the method of conformal transformation. The approach was validated against measurement and 3D electromagnetic modeling using MAFIA as well. The analysis is unique and accurate, and it is hoped that the simple approach would be of ample use and create interest to the millimeter-wave community.

Acknowledgement Authors are thankful to Dr. Lalit Kumar for a critical review of the manuscript. Authors are also thankful to Professor B. N. Basu and Dr. K. S. Bhat for many valuable suggestions.

References

1. H. Yin, G. YuBin, W. YuanYu, L. ZhiGang, H. MingZhi, and W. WenXiang, Modified tunneladder slow-wave structures for high-power millimeter-wave TWTs. Int. J. Infrared Millim. Waves **28**, 1–12 (2007).
2. J. Cai, J. Feng, X. Wu, Y. Hu, B. Qu, M. Huang, and S. Ma, Analysis and test preparation of attenuator for W-band folded waveguide TWT, in *Proceedings of the IEEE International Vacuum Electronics Conference*, Japan, 2007, pp 55–56.
3. B. Qu, J. Feng, J. Cai, and M. Zhang, Simulation of FWG TWT attenuator using Microwave Studio and MAFIA, in *Proceedings of the IEEE International Vacuum Electronics Conference*, Japan, 2007, pp. 75–76.
4. Y. N. Pchelnikov, and V. A. Solntsev, BWO with an amplifying section, in *Proceedings of the IEEE International Vacuum Electronics Conference*, 2004, pp. 73–74.
5. H. J. Ha, S.-S. Jung, and G. S. Park, Linear theory of folded-waveguide traveling-wave tubes. Journal of Korean Physics Society **34**, 297–300 (1999).
6. R. G. Carter, An improved equivalent circuit model of folded-waveguide slow-wave structures, in *Proceedings Conference on Displays and Vacuum Electronics (ITG-VDE)*, Garmisch-Partenkirchen, Germany, 2001.
7. S.-T. Han, J.-II Kim, and G. S. Park, Design of folded waveguide traveling-wave tube. Microw Opt Technol Lett **38**, 161–165 (2003).
8. B. Bhat, and S. K. Koul, *Stripline-like Transmission Lines for Microwave Integrated Circuits*. (Wiley Eastern Limited, New Delhi, 1989).
9. E. Glass, Suppression of spurious modes in high-power traveling-wave tubes. IEEE Transactions on Electron Devices **ED-30**, 1798–1806 (1983).
10. J. H. Booske, M. C. Converse, C. L. Kory, C. T. Chevalier, D. A. Gallagher, K. E. Kreischer, V. O. Heinen, and S. Bhattacharjee, Accurate parametric modeling of folded waveguide circuits for millimeter-wave traveling wave tubes. IEEE Transactions on Electron Devices **ED-52**, 685–693 (2005).
11. R. G. Carter, and L. Shunkang, Method for calculating the properties of coupled-cavity slow-wave structures from their dimensions. IEE Proc H Microw Antennas Propag **133**, 330–334 (1986).
12. N. Marcuvitz, *Waveguide handbook*. (Peter Peregrinus Ltd., London, 1986).
13. M. Genack, S. Bhattacharjee, J. Booske, C. Kory, S.-J. Ho, D. Van Der Waide, L. Ives, and M. Read, Measurements of microwave electrical characteristics of folded-waveguide circuits, in *Proceedings of the IEEE International Vacuum Electronics Conference*, California, 2004, pp. 96–97.
14. R. E. Collin, *Foundations for Microwave Engineering*. (IEEE Press, New York, 2001).